

General recipe for flatbands in photonic crystal waveguides

Omer Khayam, Henri Benisty

▶ **To cite this version:**

Omer Khayam, Henri Benisty. General recipe for flatbands in photonic crystal waveguides. Optics Express, 2009, 17 (17), pp.14634-14648. 10.1364/OE.17.014634 . hal-00567027

HAL Id: hal-00567027

https://hal-iogs.archives-ouvertes.fr/hal-00567027

Submitted on 4 Mar 2013

HAL is a multi-disciplinary open access archive for the deposit and dissemination of scientific research documents, whether they are published or not. The documents may come from teaching and research institutions in France or abroad, or from public or private research centers.

L'archive ouverte pluridisciplinaire **HAL**, est destinée au dépôt et à la diffusion de documents scientifiques de niveau recherche, publiés ou non, émanant des établissements d'enseignement et de recherche français ou étrangers, des laboratoires publics ou privés.

General recipe for flatbands in photonic crystal waveguides

Omer Khayam* **and Henri Benisty**

Nanophotonics and Electromagnetism Group, Laboratoire Charles Fabry de l'Institut d'Optique, CNRS, Univ Paris-Sud, 2 Av. Augustin Fresnel, RD 128, 91127 Palaiseau, France
**Corresponding author: omer.khayam@institutoptique.fr*

Abstract: We present a general recipe for tailoring flat dispersion curves in photonic crystal waveguides. Our approach is based on the critical coupling criterion that equates the coupling strength of guided modes with their frequency spacing and results in a significant number of the modes lying collectively in the slow-light regime. We first describe the critical coupling scheme in photonic crystal waveguides using a simple coupled mode theory model. We also determine that canonical photonic crystal waveguides natively correspond to strongly coupled modes. Based on these analyses, our design recipe is as follows: Tune the profile of the first Fourier component of the waveguide periodic dielectric boundary to lower the coupling strength of the guided modes down to its critical value. We check that this generalized tuning may be accomplished by adjusting any desired optogeometric parameter such as hole size, position, index etc. We explore the validity of this general approach down to the narrow two-missing rows waveguides. The interest of this method is to circumvent most of the common trial-and-error procedures for flatband engineering.

©2009 Optical Society of America

OCIS codes: (130.5296) Photonic crystal waveguides, (999.9999) Slow light, (260.2030) Dispersion

References and links

1. H. Kurt, H. Benisty, T. Melo, O. Khayam, and C. Cambournac, "Slow-light regime and critical coupling in highly multimode corrugated waveguides," J. Opt. Soc. B **25**, C1-C14 (2008).
2. M. Povinelli, S. Johnson, and J. Joannopoulos, "Slow-light, band-edge waveguides for tunable time delays," Opt. Express **13**, 7145 (2005).
3. T. Baba, "Slow light in photonic crystals," Nature Photon. **2**, 465 (2008).
4. T. F. Krauss, "Slow light in photonic crystal waveguides," J. Phys. D: Appl. Phys. **40**, 2666-2670 (2007).
5. M. Notomi, K.Yamada, A. Shinya, J. Takahashi, and I. Yokoyama, "Extremely large group velocity dispersion of line-defect waveguides in photonic crystal slabs," Phys. Rev. Lett. **87**, 253902 (2001).
6. H. Gersen, T. J. Karle, J. P. Engelen, W. Bogaerts, J. P. Korterik, N. F. van Hulst, T. F. Krauss, and L. Kuipers, "Real-space observation of ultraslow light in photonic crystal waveguides," Phys. Rev. Lett. **94**, 073903 (2005).
7. Y. A. Vlasov, M. O'Boyle, H. F. Hamman, and S. J. McNab, "Active control of slow light on a chip with photonic crystal waveguides," Nature **438**, 65-69 (2005).
8. A. Y. Petrov and M. Eich, "Zero dispersion at small group velocities in photonic crystal waveguides," Appl. Phys. Lett. **85**, 4866-4868 (2004).
9. S. Kubo, D. Mori, and T. Baba, "Low-group-velocity and low-dispersion slow light in photonic crystal waveguides," Opt. Lett. **32**, 2981-2983 (2007).
10. L. H. Frandsen, A. V. Lavrinenko, J. Fage-Pedersen, and P. I. Borel, "Photonic crystal waveguides with semi-slow light and tailored dispersion properties," Opt. Express **14**, 9444-9450 (2006).
11. J. Li, T. P. White, L. O'Faolain, A. Gomez-Iglesias, and T. F. Krauss, "Systematic design of flat band slow light in photonic crystal waveguides," Opt. Express **16**, 6227-6232 (2008).
12. M. Ebnali-Heidari, C. Grillet, C. Monat, and B. J. Eggleton, "Dispersion engineering of slow light photonic crystal waveguides using microfluidic infiltration," Opt. Express **17**, 1628-1635 (2009).
13. M. Mulot, A. Säynätjoki, S. Arpiainen, H. Lipsanen, and J. Ahopelto, "Slow light propagation in photonic crystal waveguides with ring-shaped holes," J. Opt. A: Pure Appl. Opt. **9**, S415-S418 (2007).
14. Y. Hamachi, S. Kubo, and T. Baba, "Slow light with low dispersion and nonlinear enhancement in a lattice-shifted photonic crystal waveguide," Opt. Lett. **34**, 1072-1074 (2009).
15. J. Ma and C. Jiang, "Demonstration of Ultraslow Modes in Asymmetric Line-Defect Photonic Crystal Waveguides," IEEE Photon. Technol. Lett. **20**, 1237-1239 (2008).

#110813 - $15.00 USD Received 30 Apr 2009; revised 22 May 2009; accepted 23 May 2009; published 4 Aug 2009

16. T. Baba, D. Mori, K. Inoshita, and Y. Kuroki, "Light Localizations in Photonic Crystal Line Defect Waveguides," IEEE J. Sel. Top. Quantum. Electron. **10**, 484-491 (2004).
17. D. Mori and T. Baba, "Wideband and low dispersion slow light by chirped photonic crystal coupled waveguide," Opt. Express **13**, 9398-9408 (2005).
18. D. Rosenblatt, A. Sharon, and A. A. Friesem, "Resonant grating waveguide structures," J. Quantum Electron. **33**, 2038-2059 (1997).
19. O. Khayam, C. Cambournac, H. Benisty, M. Ayre, R. Brenot, G. H. Duan, and W. Pernice, "In-plane Littrow lasing of broad photonic crystal waveguides," App. Phys. Lett. **91**, 041111 (2007).
20. S. Olivier, M. Rattier, H. Benisty, C. J. M. Smith, R. M. De La Rue, T. F. Krauss, U. Oesterle, R. Houdré, and C. Weisbuch, "Mini stopbands of a one-dimensional system: the channel waveguide in a two-dimensional photonic crystal," Phys. Rev. B **63**, 113311 (113311-113316) (2001).
21. H. Benisty, "Single-material coupling-tolerant semi-planar microresonator using Littrow diffraction," PNFA (2009).
22. A. Yariv, "Coupled mode theory for guided wave optics," J. Quantum Electron. **9**, 919-933 (1973).
23. H. Benisty, "Modal analysis of optical guides with two-dimensional photonic band-gap boundaries," J. Appl. Phys. **79**, 7483-7492 (1996).
24. M. L. Cohen and T. K. Bergstresser, "Band Structures and Pseudopotential Form Factors for Fourteen Semiconductors of the Diamond and Zinc-blende Structures," Phys. Rev. **141**, 556 (1966).
25. O. Khayam, H. Benisty, and C. Cambournac, "Experimental observation of minigap stripes in periodically corrugated broad photonic wires," Phys. Rev. B **78**, 153107 (2008).
26. W. T. Lau and S. Fan, "Creating large bandwidth line defects by embedding dielectric waveguides into photonic crystal slabs," Appl. Phys. Lett. **81**, 3915 (2002).
27. Y. A. Vlasov, N. Moll, and S. J. McNab, "Mode mixing in asymmetric double-trench photonic crystal waveguides," J. Appl. Phys. **95**, 4538 (2004).
28. S. G. Johnson, M. Povinelli, M. Soljacic, A. Karalis, S. Jacobs, and J. Joannopoulos, "Roughness losses and volume-current methods in photonic-crystal waveguides," Appl. Phys. B **81**, 283-293 (2005).
29. C. Vassallo, "About coupled-mode theories for dielectric waveguides," IEEE J. Lightwave Technol. **6**, 294-303 (1988).
30. D. Mori and T. Baba, "Dispersion-controlled optical group delay device by chirped photonic crystal waveguides," Appl. Phys. Lett. **85**, 1101-1103 (2004).
31. B. M. Möller, U. Woggon, and M. V. Artemyev, "Band Formation in Coupled-Resonator Slow-Wave Structures," Opt. Express **15**, 17362-17370 (2007).
32. M. Notomi, E. Kuramochi, and T. Takasumi, "Large-scale arrays of ultrahigh-Q coupled nanocavities," Nature Photon. **2**, 741-747 (2008).
33. J. Jágerská, N. Le Thomas, V. Zabelin, R. Houdré, W. Bogaerts, P. Dumon, and R. Baets, "Experimental observation of slow mode dispersion in photonic crystal coupled-cavity waveguides," Opt. Lett. **34**, 359-361 (2009).
34. D. Englund, I. Fushman, and J. Vuckovic, "General recipe for designing photonic crystal cavities," Opt. Express **13**, 5961-5976 (2005).
35. H. Benisty, "Graphene nanoribbons: Photonic crystal waveguide analogy and minigap stripes," Phys. Rev. B **79**, 155409 (2009).

1. Introduction

A simple wavelength-scale periodic boundary corrugation along a dielectric waveguide confers it the extraordinary ability to slow down light [1, 2]. Waveguides made out of 2D periodic photonic crystal (PhC) lattice are no exception in this regard [3-7] and in addition to the peculiarities of a 1D periodic propagation, they offer a 2D photonic bandgap (PBG) guiding mechanism. The slow light regime in a PhC waveguide corresponds to obtaining a "flatband"– a region of the dispersion relation where the mode has a zero or constant group velocity v_g, extending over a fraction of the *k*-space around the first Brillouin zone (BZ) edge. In practice, however, the bands of an actual PhC waveguide only form a local extrema at the BZ edge and the extent of the slow v_g region is very limited. One inherent reason for this is the hyperbolic character of the waveguide dispersion relation that fundamentally limits the span of the flatband inside the BZ. The other more extrinsic and less documented reason, as we shall learn, is the unadapted coupling behavior of the basic waveguide modes. It is the strength 'κ' of this modal interaction that shapes the waveguide dispersion bands and causes a canonical *n*-missing rows PhC waveguide (a so-called W*n*) to lie, by default, in the non-flatband regime.

Recently, several waveguide designs have been proposed to achieve flatband slow light based on tuning structural parameters such as the size of the boundary holes [8-10], their position [11], their refractive index [12, 13], the waveguide symmetry [14, 15] and chirping

#110813 - $15.00 USD Received 30 Apr 2009; revised 22 May 2009; accepted 23 May 2009; published 4 Aug 2009
(C) 2009 OSA

the PhC waveguide [16, 17]. While each approach has its merits for the purpose it serves, a general recipe for flatband tailoring seems absent. Also the studies mentioned above are for particular monomode PhC waveguides, namely W1 and W2, it is unclear how they can be extended to more general waveguide widths. It is equally important to understand the band formation mechanism inside the PBG of PhC waveguides. This article aims at unifying these approaches under a common framework. It is admittedly difficult to relate *ab initio* the band flatness to the dielectric map of narrow W*n* waveguides. But based on the findings of [1], we find it profitable to expand the problem as the obtainment of flatness in broader multimode waveguides. We find that this leads to a simple universal criterion when employing an analysis on basic guided modes familiar to coupled-mode theory (CMT) practitioners. In this paper, we devise a recipe based on this criterion and validate it towards narrower waveguides as much as possible.

To situate our approach, we start with a qualitative description of the fundamental slow light mechanisms in the rich framework of PhC waveguides. Apart from laterally confining modes by the PBG effect, the periodic waveguide cladding also acts a grating, giving rise to "resonant diffraction" [18] of certain guided modes. These resonant conditions appear as zero-group-velocity points on the dispersion diagram. Figure 1 categorizes the three basic types of slow light processes in a PhC waveguide and relates them to their standing oscillation patterns using the familiar ray picture. The flatband at $k_z = 0$ in the band diagram (point '1' in Fig. 1(b)) corresponds to the conventional Fabry–Perot (FP) mode that draws its feedback from specular reflections from the waveguide boundary. As shown in Fig. 1(a) such an oscillation is purely transverse. At the first BZ edge ($k_z = \pi/\Lambda$), a forward-propagating guided mode a_m of order m couples to its backward-propagating counterpart b_m producing an anticrossing – a gap with two band extrema, referred as '2' in Fig. 1. From a diffraction perspective, the BZ-edge zero v_g modes at each extrema satisfy the Littrow condition and are retro-diffracted back along the incident path. The PhC cladding, in this case, acts as a 'distributed Littrow reflector' providing feedback for the obliquely resonant "Littrow modes" [19]. The third type of slow light mechanism occurs inside the BZ where contrapropagating modes of *different* orders, namely m and m', interact. At a point in the *k*-space where their phase matching condition is satisfied, anticrossings or minigaps form [20], referred to as '3' in Fig. 1(b). Figure 1(a) shows the oscillation pattern at such a resonant anticrossing condition. If it occurs closer to the BZ-edge, the modes are called "near-Littrow modes" [19]. In mechanisms 2 and 3, the guided mode at band extrema of the anticrossing diffract either into itself or into another mode forming a stationary interference pattern or the *slow mode*. The width $\Delta\omega$ of the anticrossing in either case is dictated by the coupling strength κ and is given by $\Delta\omega = 4\kappa c / \left(n_g^a + n_g^b\right)$, where n_g is the group index of the modes and *c* the light velocity in vacuum.

To produce a 'flatband' based on the above picture, we proceed as follows: Consider, for example, the blue branch from anticrossing '2' to anticrossing '3' in Fig. 1(b). If the widths of the two anticrossings are simultaneously increased, the two ends of the considered branch would move in opposite frequency directions: point A descends and point B rises until the curvature of the branch approaches zero and a flatband is formed, as shown in Fig. 1(c). So, we infer that the band flatness results from the *interaction* of at least two anticrossings. This makes the coupling strength κ a natural design parameter in any band engineering approach. The extension of the above scheme leads us to consider a *multimodal interaction* where several flatbands can be formed by managing all the anticrossings as coherently as possible. In this work, based on the above remarks, we shall demonstrate how by tuning the width of the anticrossings through any generic engineering of κ, the dispersion relation can be tailored to deterministically produce a flatband.

For the sake of completeness here, we briefly highlight in Fig. 1(d) the significance of the flatband situation with respect to the Littrow resonances at and near the BZ edge. The large Δk_z range of the flatband (see Fig. 1(c)) translates into a large angular bandwidth $\Delta\theta$, over which the mode does not apparently disperse and retains its resonant character. This is actually made possible by the hybridization of the Littrow mode with the other interacting

#110813 - $15.00 USD Received 30 Apr 2009; revised 22 May 2009; accepted 23 May 2009; published 4 Aug 2009
(C) 2009 OSA

near-Littrow modes like type '3' of Fig. 1(a). The ray picture does indeed suggest that, starting from Littrow condition of type '2', the optical path is stationary at first order in $\Delta\theta$ when evolving to the type '3' situation. There are some practical implications to this, such as, for instance angular tolerance for coupling into slow modes of a waveguide resonator [21]. We shall, however, use only the *k*-space band description of slow light in this paper. In the following section, the theory of the critical coupling is elaborated using conventional CMT models. Section 3 discusses the design approach for achieving critical coupling in PhC waveguides.

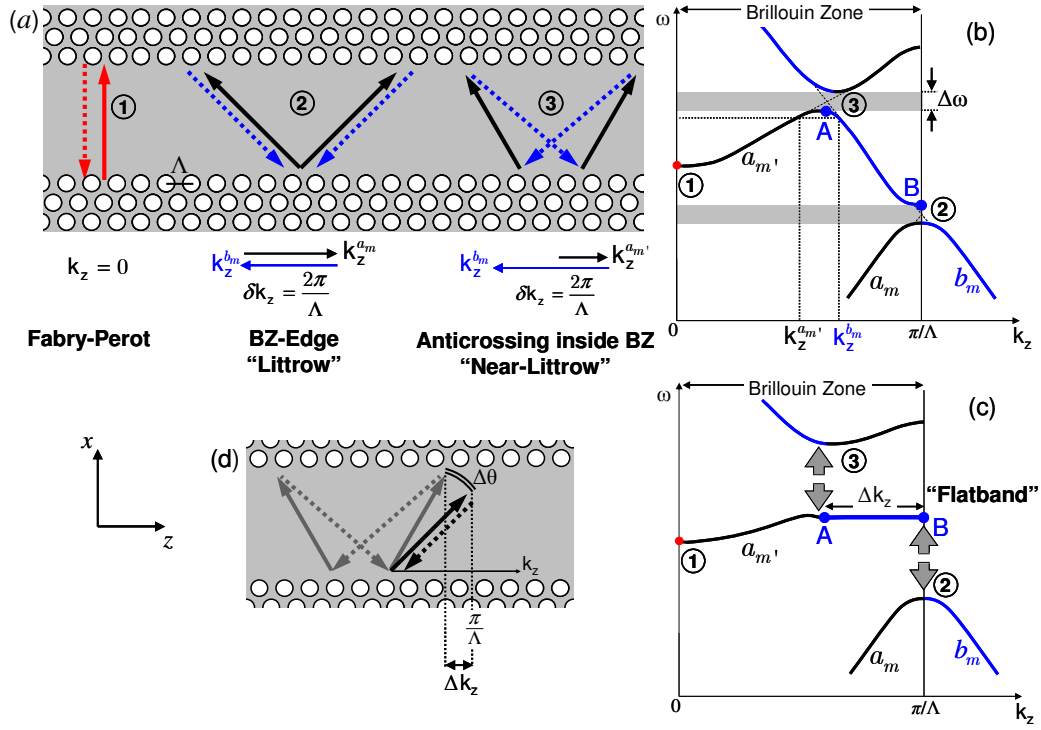


Fig. 1. Slow light mechanisms in PhC waveguide. (a) Oscillation patterns of 1. Fabry-Perot, 2. BZ-edge Littrow and 3. inside-BZ anticrossing modes and (b) their positions on a schematic dispersion diagram. (c) A flatband is formed near BZ edge by increasing the coupling strength κ, and hence the gap width $\Delta\omega_{ab}$, at anticrossings 2 and 3. (d) The spread Δk_z of the flatband corresponds to the slow mode angular bandwidth $\Delta\theta$ inside the waveguide. The arrows show the resonance path of the flatband mode at BZ-edge (black arrows) and near BZ-edge (grey arrows).

2. Critical coupling phenomenon in multimode interaction

The modal interaction in a periodic structure can analytically be described by conventional coupled mode theory (CMT) [22]. In our recent study [1], we extended the coupled mode formalism to the case of coupling between multiple contrapropagating modes in broad dielectric waveguides with a periodically corrugated boundary. In such a multimodal environment it is the coupling coefficient κ that, although acting locally between two modes, affects the global shape of the bands. Figure 2 shows the evolution of a generic multimode band structure of equidistant modes with increasing coupling strength, as calculated from the CMT: Here we consider four forward and backward modes with a constant free spectral range (FSR) and uniform coupling, i.e. constant κ. The no-coupling case ($\kappa = 0$) represents an "empty lattice" system where the native uncoupled modes are left unperturbed. Oscillating bands are formed when mini-gaps open for nonzero κ values and initially increase in width as

#110813 - $15.00 USD Received 30 Apr 2009; revised 22 May 2009; accepted 23 May 2009; published 4 Aug 2009
(C) 2009 OSA

κ increases. However, when the gaps are of the same order of magnitude as the FSR (Fig. 2(c)), the bands flatten. The corresponding value of the coupling coefficient is called the critical coupling, 'κ_c' , and scales precisely as FSR/π [1] (wavevectors and frequencies are related by the canonical group velocity of the problem). Beyond the critical coupling point, the bands revert to their original shape below critical coupling, with the exception of one less minigap (band oscillation). It can be remarked that critical coupling does leave some residual oscillations at the edges of the interaction region, not discussed in depth here.

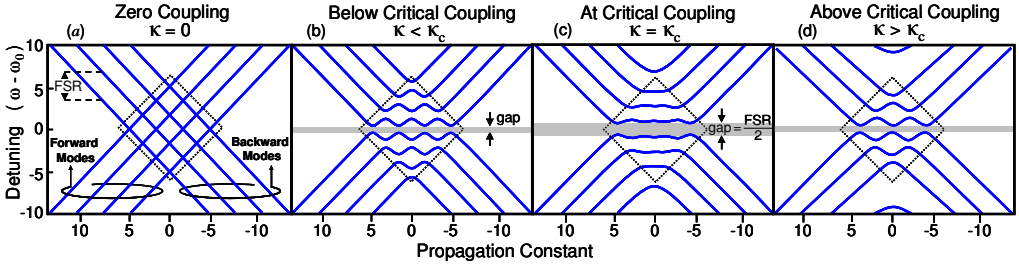


Fig. 2. Evolution of equidistant and linear bands with increase in coupling strength. The interaction region is enclosed in a lozenge (dotted lines). At critical coupling, the gap width increases to half of the FSR.

It is the simplicity of these ingredients (equidistant and linear mode branches, as shown in Figure 2) that we exploit here to introduce the concept of critical coupling. In what follows, we describe a framework to look at critical coupling in the modified context of hyperbolic dispersion relations, as is the case in PhC waveguides, and study the effect of varying modal coupling strength on the band shape.

2.1 CMT model of a photonic crystal waveguide

The dispersion relation of the PBG guided modes in a PhC waveguide can effectively be modeled by CMT. The basic coupled mode equations for two sets of contradirectional propagating modes, represented by their amplitudes $a_m(z)$ and $b_{m'}(z)$, are given by:

$$\left(i\frac{d}{dz}+\delta_m^a\right)a_m(z)+\sum_{m'=0}^{N}P\,\kappa_{mm'}\,b_{m'}(z)=0,\quad \text{where } \{m\in\mathbb{Z}:0\le m\le N\} \tag{1}$$

$$\left(-i\frac{d}{dz}+\delta_{m'}^b\right)b_{m'}(z)+\sum_{m=0}^{N}P\,\kappa_{mm'}\,a_m(z)=0,\quad \text{where } \{m'\in\mathbb{Z}:0\le m'\le N\} \tag{2}$$

where m and m' are the mode orders of the forward and backward modes of native dispersions δ_m^a and δ_m^b respectively, *N* the total number of modes and *P* is the parity condition depending on the waveguide symmetry. Note that we shall use the words 'modes' and 'branches' interchangeably here. In a grating waveguide with only one of its boundaries corrugated, each forward-propagating mode interacts with a backward-propagating-mode and the parity variable has a fixed value of *P* = 1. However, when both the opposite boundaries are corrugated about a symmetry plane, as is the case in a canonical PhC waveguide, only similar parity modes interact [23] – a forward-propagating *even* mode couples with a backward-propagating mode of *even* parity only. The parity condition is then defined as $P=\left|(-1)^m+(-1)^{m'}\right|/2$ (unity or zero).

The hyperbolic dispersion of the native modes of a generic perfect-wall waveguide can be incorporated into the CMT model by the dispersion $\delta_m^a=\sqrt{\beta_m^2-\left(mFSR_0\right)^2}$ for the forward modes and $\delta_{m'}^b=\sqrt{\beta_m^2-\left(m'FSR_0\right)^2}-2\Delta$ for the folded backward modes where

#110813 - $15.00 USD Received 30 Apr 2009; revised 22 May 2009; accepted 23 May 2009; published 4 Aug 2009
(C) 2009 OSA

$\beta = n_g \omega / c$. FSR_0 is the hyperbolic branch frequency-spacing at $\delta_m^a = 0$ (the wavevector of FP modes), often expressed in terms of the waveguide width W as π / W . The parameter Δ corresponds to the first Brillouin zone edge symmetry point where the forward and backward branches, related by the first Fourier component of the periodicity, intersect one another. Such a mode coupling description relaxes the need for an explicit definition of Bragg frequencies as well as periodicity of the system. We assume all modes interact with the same strength, thus $\kappa_{mm'} = \kappa$ for all m and m'. The success of so simple an assumption will be seen later. The coupled mode equations can be cast into a matrix form as below:

$$\frac{d}{dz} M = iC M \tag{3}$$

where M is a vector of $2N$ elements containing the mode amplitudes in the order $M = (a_1, b_1, a_2, b_2, \ldots, a_N, b_N)^T$, where T denotes the transpose. C is the coupling matrix with frequency detuning along the diagonal $C_{2m+1,2m+1} = -\delta_m^a$ (forward modes, Eq. (1)) and $C_{2m'+2,2m'+2} = \delta_{m'}^b$ (backward modes, Eq. (2)) and coupling coefficients as off-diagonal elements such that, $C_{2m+1,m'+2} = -\kappa$ and $C_{2m+2,m'+1} = \kappa$ for the odd and even rows respectively. All other matrix elements are zero to cancel co-directional couplings. For each frequency of interest (the vertical axis), we diagonalize the matrix C and obtain the eigenvalues $i\gamma$ which are the wavevectors with real part Re(γ) corresponding to the propagating modes and imaginary part Im(γ) representing the evanescent modes.

Describing a periodically corrugated waveguide by such a CMT model is analogous to the pseudo-potential method [24] used so often in solid-state physics to calculate the electronic band structures based on empirical Fourier coefficients values for the periodic crystal potential. In the CMT model, the periodic index modulation of the optical waveguide system, with or without a PBG, is quantified in terms of the coupling strength κ of the guided modes and is used to calculate the approximate dispersion relation. Figures 3(a)-3(c) shows the CMT results for three cases of mode coupling. When $\kappa = 0$, as in the case of a simple uncorrugated dielectric waveguide, no modal coupling occurs and the artificially folded bands simply cross one another as shown in Fig. 3(a). This region of overlapping forward-backward branches is symmetrically spread around point Δ and, as shall be seen, it is here that the intermodal interaction shapes the band dispersion. Notice that the spacing FSR_0 of the branches is constant at $k_z \equiv$ Re(γ) = 0, whereas at the band folding point Δ, the modal spacing that we may denote FSR_Δ, gradually increases from lower to higher β.

For non-zero values of κ, Figs. 3(b) and 3(c), the crossings convert to anticrossings and curly bands are formed respecting their parity conditions: Figure 3(b) is the typical case of a parity independent coupling ($P = 1$ in Eqs. (1)-(2)) where each crossing forms an anticrossing. This band structure is representative of a single-side corrugated waveguide such as a "single-trench (ST) PhC waveguide" (see Fig. 5), where an air trench replaces a single row of holes on one of its boundaries. In section 3, we shall use them to study flatband formation in PhC waveguides under the critical coupling regime. In Fig. 3(c), parity-dependent coupling, as in the case of a canonical PhC waveguide with regular round holes and a central symmetry plane [23], causes the dispersion bands to roll up like necklaces separated by so-called "stripes of minigaps" [25]. The band diagram of an actual PhC waveguide W7, calculated using plane wave expansion (PWE) method, is plotted in Fig. 3(d) for comparison. It is clear that the CMT model mimics all the band structure features arising from the coupling behavior of the PBG-guided modes in a PhC waveguide. The only difference being the continuum of dielectric and air bands which is naturally absent from the CMT picture. We may add that in an actual PhC waveguide, the FSR at k_z=0 varies slightly with the modal frequency and angle due to periodic width modulation at the boundaries. This aspect, although not taken directly into account here in the CMT model, does not affect the coupling behavior of modes at the BZ edge.

#110813 - $15.00 USD Received 30 Apr 2009; revised 22 May 2009; accepted 23 May 2009; published 4 Aug 2009
(C) 2009 OSA

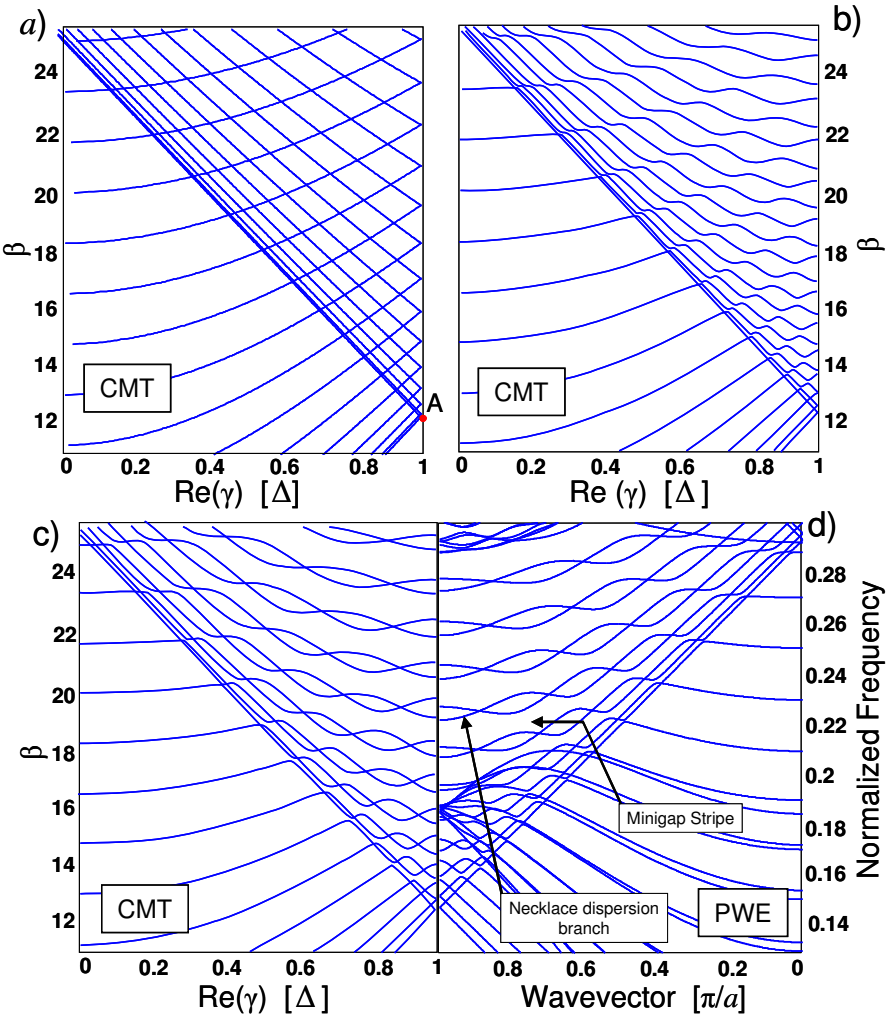


Fig. 3. (*a*-c) Dispersion diagrams at different coupling coefficient values obtained from the CMT model of PhC waveguide modes. (*a*) $\kappa = 0$ case (b) $\kappa > 0$ case with parity-independent and (c) parity-dependent coupling (d) actual W7 raw dispersion diagram calculated with the PWE supercell method (only the discretization of PhC air and dielectric bands depends on the supercell size). The minigap-stripes and the necklace dispersion branches are perfectly mimicked by the CMT model.

2.2 Flatbands at critical coupling

Using the above developed CMT model, we now examine the effect of increasing the modal interaction strength on the hyperbolic bands, up to the point where the coupling coefficient is of the same order of magnitude as the FSR. We consider a general multimode case where FSR_0 is taken as unity and the mode orders are in the range of $0 \le m \le 28$. The value of κ is kept uniform throughout the coupling matrix *C*, i.e. all modes couple with the same strength with all modes of opposite direction, whether $m = m'$ or $m \ne m'$. At the critical coupling value κ_c, the dispersion diagram manifests a region centered around the BZ edge (point Δ) where the local band oscillations are almost null. The red lozenge in Fig. 4 encloses the vertical and horizontal extent of this flatband region. The dispersion diagrams for both parity-dependent (Fig. 4(a)) and parity-independent (Fig. 4(b)) cases are extended into the second BZ ($\Delta < \mathrm{Re}(\gamma) < 2\Delta$) to reveal the full extent of the forward-backward coupling region

#110813 - $15.00 USD Received 30 Apr 2009; revised 22 May 2009; accepted 23 May 2009; published 4 Aug 2009
(C) 2009 OSA

around the first BZ edge. It is clear that the flatband region occurs in the interval $15 \leq \beta \leq 21$, while the bands above and below it retain their oscillatory profile. The localized occurrence of the critical coupling is logically explained from the fact that the FSR_Δ is not uniform but increases gradually from point A onwards to higher frequencies. In our case, the average FSR_Δ in the red lozenge is approximately ~ 0.76 and the critical coupling occurs at $\kappa_c = FSR_\Delta / \pi = 0.242$ in the parity-independent case and at twice that value in the parity-dependent case. Since only similar parity modes couple in the later case, the anticrossings widths, and hence κ_c, are twice as large as the former case. Also evident from Fig. 4 is the difference between the flatbands of the two parity schemes. In Fig. 4(a), the effect of critical coupling is to 'squeeze' the necklace bands and widen the minigap-stripes. In Fig. 4(b) the bands smooth out more evenly. For the sake of clarity, in section 3 we shall employ the parity-independent band structures of an ST-PhC waveguide to demonstrate flatband engineering in PhC waveguides.

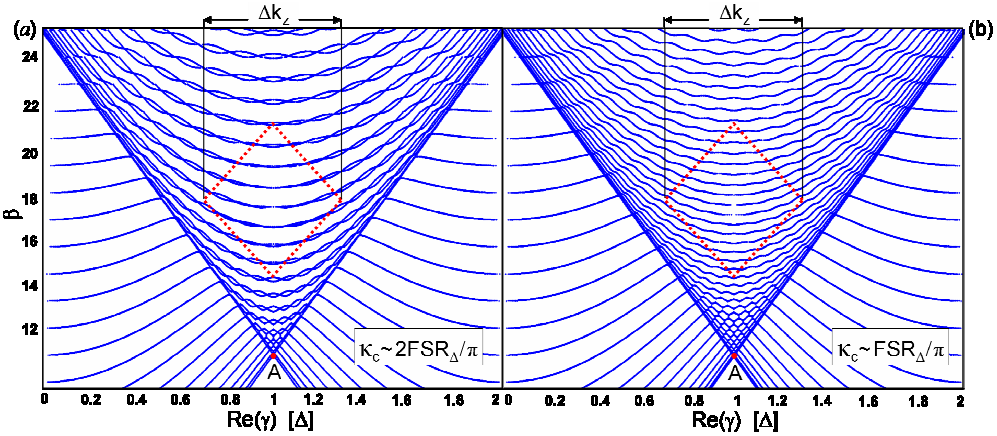


Fig. 4. Dispersion diagrams at critical coupling in (a) parity-dependent and (b) parity-independent schemes. The red lozenge encloses the flatband region. FSR_Δ inside the lozenge is approximately 0.75 in (a) and 0.375 in (b), FSR_0 being taken as unity.

2.3 Features and limits of critically-coupled flatbands

A striking feature of the critical coupling is the significant number of modes collectively lying in the slow-light regime. The β-range of the flatband region depends on the FSR_Δ variation along frequency. For the case of coupling among linear branches (see Fig. 2) the FSR_Δ variation being absent, all interacting modes achieve critical coupling simultaneously. Along the abscissa, the flatband region occurs in a wavevector window $\Delta k_z \equiv \Delta[\mathrm{Re}(\gamma)]$ around point Δ, as shown in Fig. 4. In our case of multiple bands, it can be defined as the k_z interval in which a given band centered at Δ, rises by an FSR_Δ. As evident in Fig. 4, its indefinite extension to the entire BZ is restricted primarily by the intrinsic hyperbolic curvature of the waveguide dispersion relation. Interestingly, even when the coupling coefficient is uniform ($\kappa_{mm'} = \kappa$) for all mode branches, the anticrossings formed are not all of the same size. This makes the minigap-stripes symmetrically narrow down away from the first BZ edge – a feature also visible in the actual PhC waveguide dispersion relation in Fig. 3(d). This implies that tailoring Δk_z may theoretically be possible by individually changing local anticrossing widths with a nonuniform spread of coupling coefficients. Inside the Δk_z window , the number of oscillations per band scales inversely with the square root of the waveguide width W as shown in appendix A1 of [1] . Narrower waveguides with fewer band oscillations would therefore show a wider spread of band flatness. These aspects shall also depend on the targeted application domain.

#110813 - $15.00 USD Received 30 Apr 2009; revised 22 May 2009; accepted 23 May 2009; published 4 Aug 2009
(C) 2009 OSA

3. Achieving critical coupling in photonic crystal waveguides

In order to physically achieve critical coupling in a periodically corrugated photonic wire such as a PhC waveguide, we need to (*i*) identify a design parameter to access and tune the coupling strength of its guided modes and (*ii*) assess the 'default' state of this strength that, in the specific case of a canonical PhC waveguide, we shall find to be 'overcoupled'. The two points are elaborated below.

In a corrugated waveguide, each guided mode has a nonzero overlap with the cladding's modulated region as shown in Fig. 5(d). In CMT, it is this overlap that essentially dictates the coupling strength κ_{ab} between a forward mode a_m of order m and a backward mode $b_{m'}$ of order m', given by:

$$\kappa_{ab} = \frac{k_0^2}{2k_z}\frac{\int E_a(x)E_b(x)\hat{\varepsilon}_1(x)\mathrm{d}x}{\int E_a(x)E_b(x)\mathrm{d}x} = \frac{k_0^2}{2k_z}\Gamma_x = \frac{2\pi}{\Lambda}u^2\Gamma_x \qquad (4)$$

where $u=a/\lambda=\omega a/2\pi c$ is the normalized frequency (allowing to correspondingly introduce FSR_u) and Λ the period. Here a scalar version is given for simplicity and the BZ edge is considered. Γ_x is the normalized overlap integral of the *unperturbed* modal intensity profile, $E_m(x)E_{m'}(x) = |E(x)|^2$, with the first Fourier harmonic of the boundary dielectric profile $\hat{\varepsilon}_1(x) = \mathrm{FT}[\varepsilon(x,z)] = (2\pi)^{-1}\int \varepsilon(x,z)\exp(iG_o z)\,dz$, where $G_o = (2\pi/\Lambda)$. We argue that a PhC waveguide satisfies this description when operated inside the bandgap. The physical reason, as pictured in Fig. 5(d) is the strong decay of the modal field in the periodic PhC cladding. Strong refractive-index contrast is of course a crucial factor for this rapid decay, as it is for the omnidirectionality of PhC bandgap. For our purpose, it means that the overlap integral Γ_x appearing in Eq. (4) has sizable contribution from only the first or second rows adjacent to the core. In other words, only the first few lobes of the dielectric Fourier harmonic profile $\hat{\varepsilon}_1(x)$ in Fig. 5(d) are of interest.

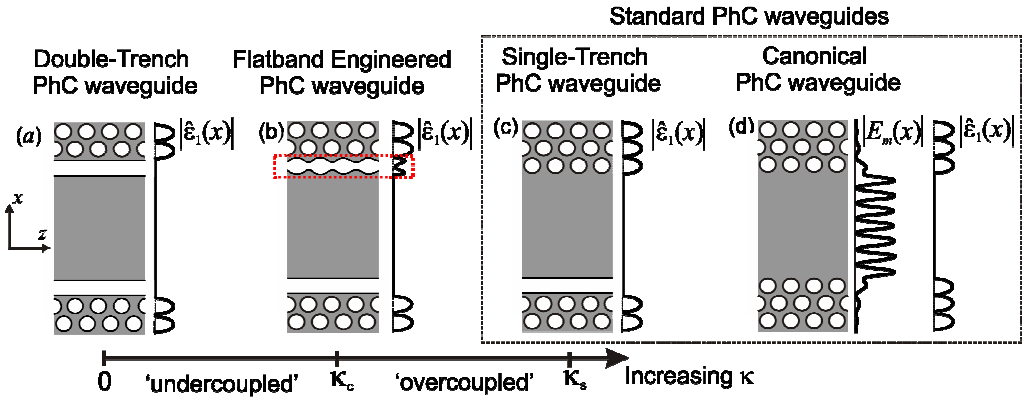


Fig. 5. Classification of PhC waveguide variants according to their coupling strength as compared to that of the uncoupled DT-PhC waveguide modes.

Based on the graphical analysis in appendix A, Fig. 5 shows a general classification of the PhC waveguide structures according to their coupling strength κ. At the lower end is the double-trench (DT) PhC waveguide, shown in Fig. 5(a) along with its first Fourier component dielectric profile $\hat{\varepsilon}_1(x)$, where the first row of air holes at both the boundaries is replaced by air trenches. The absence of the boundary component of $\hat{\varepsilon}_1(x)$ almost kills the modal coupling, that is $\kappa \sim 0$. Such waveguides, studied previously in [26-28], are a good approximation of the desirable 'unperturbed' PhC waveguide since they retain the PBG yet the bandgap-guided modes remain virtually uncoupled. Standard PhC waveguide structures, with regular round-shaped air holes at the boundary lie on the higher end of the κ scale,

#110813 - $15.00 USD Received 30 Apr 2009; revised 22 May 2009; accepted 23 May 2009; published 4 Aug 2009
(C) 2009 OSA

denoted by 'κ_S'. The single-trench (ST) PhC waveguide in Fig. 5(c) is simply a parity-degeneracy lifted version of the canonical PhC waveguide in Fig. 5(d). The only difference is the size of the splitting which is twice as large in the later case. The zero-dispersion flatband regime occurs at the critical coupling strength κ_c, such that $\kappa_c < \kappa_S$. From previous analysis [1], we established that in this critical regime, the dimensionless ratio κ_c / FSR_ω approaches a value of $1/\pi$. This scaling can be grasped from the fact that the frequency splitting in a standard contradirectional case is ~2κ. It can be seen from Figure 5(b) that the boundary component of $\hat{\varepsilon}_1(x)$ in the flatband waveguide, highlighted in dotted red line, is modified in amplitude and shape as compared to the standard waveguides which are comparatively 'overcoupled'. This trend suggests a general design philosophy for obtaining zero-dispersion bands – to tailor the first Fourier component profile $\hat{\varepsilon}_1(x)$ of the canonical PhC waveguide cladding so as to lower its coupling strength from κ_S to the critical coupling value κ_c. In terms of structural parameters, this translates into, for instance, changing the form, position or the index of the waveguide boundary holes as detailed below.

For the quantitative demonstration of our design strategy, we introduce here a useful quantity called the '*critical overlap*', that simply corresponds to the slowdown regime at κ_c and is deduced from Eq. (4) as,

$$\Gamma_x^{\text{critical}} = n_g FSR_u / u^2 \pi \tag{5}$$

Given an unperturbed waveguide system with mode spacing FSR_u and modal group index n_g, the critical overlap value $\Gamma_x^{\text{critical}}$ serves as a gauge for flatband engineering of its perturbed counterpart. In our analysis, we use the modal field $E(x)$ of a DT-PhC waveguide and the profile $\hat{\varepsilon}_1(x)$ of the investigated ST-PhC waveguide to calculate the overlap integral Γ_x. Here, an ST-PhC waveguide is preferred over the canonical symmetric version for the sake of clarity. The absence of parity degeneracy in such waveguides facilitates understanding of band formation (no band pairing) and has no effect on the intrinsic number of the guided modes. The optogeometric parameters are then varied in order to lower Γ_x down to $\Gamma_x^{\text{critical}}$. We also independently check that the bands do become flat for this condition, i.e. for $\Gamma_x = \Gamma_x^{\text{critical}}$, using the following criterion: We define an *average absolute velocity* $\langle |v_g| \rangle$ as the average of $|v_g|$ over a lozenge-shaped area of the band structure centered at the BZ edge, previously employed in Fig. 4. Except for slight discrepancy in ultimately confined waveguide, we will find good agreement between the critical overlap criteria and the actual achievement of slow light in the lozenge BZ edge region.

Unless otherwise specified, the PhC is defined as triangular lattice of air holes in a substrate of index 3.21 (typical of actual InP-based heterostructures) and the dispersion diagrams are calculated by PWE method. For the overlap integral, the modal field of the DT-PhC waveguide in 2D supercell is averaged along the *z*-axis. Such a 1D field is an appropriate approximation in order to focus on the first Fourier component. It is notoriously delicate to establish coupling strength in high-index contrast structures and with vector fields (see, e.g. [29], for seminal work on such aspects). In our case, the electric field *x* component becomes very strong in the trench so that $\int |E(x)|^2 dx$ can have its largest contribution from the trench alone, leading to several anomalies. We thus found it appropriate to use a DT-PhC waveguide electric field derived from the $D(x)$ field by a somewhat larger dielectric constant (typically ε_r=2.4) in the trench. In this procedure, for consistency, we choose this value by constraining the resulting field profile $|E(x)|^2$ to fit that of the ST-PhC waveguide, i.e. the average field in the presence of holes rather than a trench, an approach adapted to the optogeometric optimization space.

#110813 - $15.00 USD Received 30 Apr 2009; revised 22 May 2009; accepted 23 May 2009; published 4 Aug 2009
(C) 2009 OSA

Next we consider a few structural tuning techniques and design parameters that serve as a control handle over the modal coupling strength in PhC waveguides. While we only show a proof of principle here by optimizing the boundary contribution of $\hat{\varepsilon}_1(x)$, i.e. the first row of holes, the analysis equally applies to shaping the entire $\hat{\varepsilon}_1(x)$ distribution of the waveguide, either deeper in the cladding or in the central core.

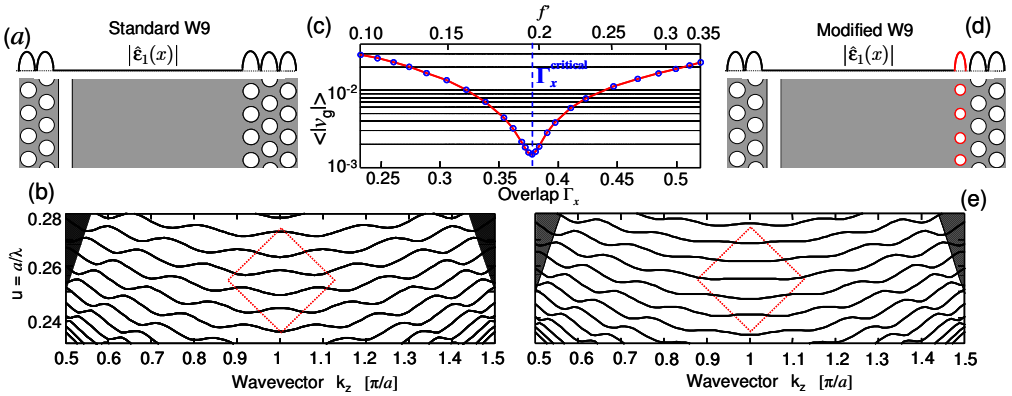


Fig. 6. (a). A standard W9 ST-PhC waveguide, its first Fourier component dielectric profile and (b) its dispersion diagram. The dark triangular regions at the corners represent the light cone. (c) Evolution of the average group velocity with the change in hole size, labeled through *f*' and through the overlap integral. The curve dips by an order of magnitude at the critical overlap value obtained from the simple Eq(5). (d) W9 ST-PhC waveguide with modified hole size and (e) its actual flattened band diagram. The flatbands are highlighted in the red lozenge, where the quantity plotted in (c) is extracted.

3.1 Hole size

Adjusting the boundary hole size for tuning the delay-bandwidth product in narrow single mode PhC waveguides (namely W1 and W2) has recently been demonstrated by several groups [8-10]. They showed that for different hole radii, the slope of the band near BZ-edge hinges on the anticrossing between the index mode and the PBG guided mode. Here we show that this approach is equivalent to changing the shape of $\hat{\varepsilon}_1(x)$ and results in critical coupling. Also, we choose a broader waveguide to show that the analysis can be extended to multimode systems. Figures 6(a)-6(b) shows a standard W9 ST-PhC waveguide, its dielectric first Fourier component distribution and its dispersion diagram. All holes are circularly shaped in a triangular lattice of fill factor $f = 0.35$. The dispersion bands are plotted in the first and second BZ to reveal the entire coupling region around the first BZ edge. Since the critical coupling occurs only locally in a (u, k_z) window around the BZ edge, we focus on a few bands enclosed inside the red lozenge in Fig. 6(b). The average normalized group velocity of these bands, conveniently defined as $\langle|\overline{v}_g|\rangle = \langle|du/dk|\rangle$, is plotted in Fig. 6(c) as a function of the design parameter *f*', the fill factor of the innermost row of PhC cladding holes. At a certain reduced hole size (*f*'=0.2), the bands collectively flatten out and $\langle|\overline{v}_g|\rangle$ dips by more than one order of magnitude. Figure 6(e) shows the respective flattened band diagram at this point. Further decreasing the hole size returns $\langle|\overline{v}_g|\rangle$ to its original value at the unmodified hole size. To relate this behavior to the modal coupling strength, we calculate the overlap Γ_x of a typical near BZ-edge mode of a W9 DT-PhC waveguide inside the lozenge, given by u=0.26 and k_z=0.95. The bottom axis in Fig. 6(c) shows Γ_x for each hole size. The critical overlap for this mode is found from Eq. (5) to be approximately $\Gamma_x^{\text{critical}}$=0.3776. This value agrees closely to the $\langle|\overline{v}_g|\rangle$ dip in Fig. 6(c) at Γ_x=0.3753. Thus by varying the spatial duty cycle of boundary index modulation, the strength of $\hat{\varepsilon}_1(x)$ can be diminished (as shown schematically

#110813 - $15.00 USD Received 30 Apr 2009; revised 22 May 2009; accepted 23 May 2009; published 4 Aug 2009
(C) 2009 OSA

in Fig. 6(d)) to achieve critical overlap. Below this value, the modes are in the undercoupled regime and collectively regain their group velocity. It may be noticed that the top scale in Fig. 6(c) is not linear due to the complex relationship of the geometrical parameter (hole size in this case) with the overlap integral. Only in the case of varying the hole epsilon, a quantity direct proportional to the overlap integral, shall we find the scales linear.

3.3 Hole epsilon

Varying the index contrast of the waveguide's periodic boundary, by either microfluidic infiltration [12] or by exploiting ring-shaped holes [13] is yet another way of optimizing $\hat{\varepsilon}_1(x)$ to achieve slow light. Figures 7(a)-7(b) shows a standard W5 ST-PhC waveguide and its dispersion diagram. Increasing the dielectric constant of the inner most row of holes, ε_{hole}, decreases the boundary contribution of $\hat{\varepsilon}_1(x)$, as shown schematically in Fig. 7(d). As in the previous case we focus on the BZ-edge bands in the red lozenge to highlight the collective slowdown effect. For the Γ_x calculations, we now use the field of the mode at u=0.2724 and k_z=0.95 of a W5 DT-PhC waveguide. Figure 7(c) shows the evolution of $\langle|\overline{v}_g|\rangle$ and Γ_x with increasing ε_{hole}. At the critical overlap, $\langle|\overline{v}_g|\rangle$ now dips by an order of magnitude. The shift between $\Gamma_x^{\text{critical}}$ value (0.6476) and the lowest $\langle|\overline{v}_g|\rangle$ point at Γ_x=0.6418 is only 1%. It may be noted that only a slight increase in hole index (ε_{hole}~1.5^2) is required to achieve the critical regime. This value corresponds qualitatively to the recent analysis in [12] but they use a narrow W1 waveguide.

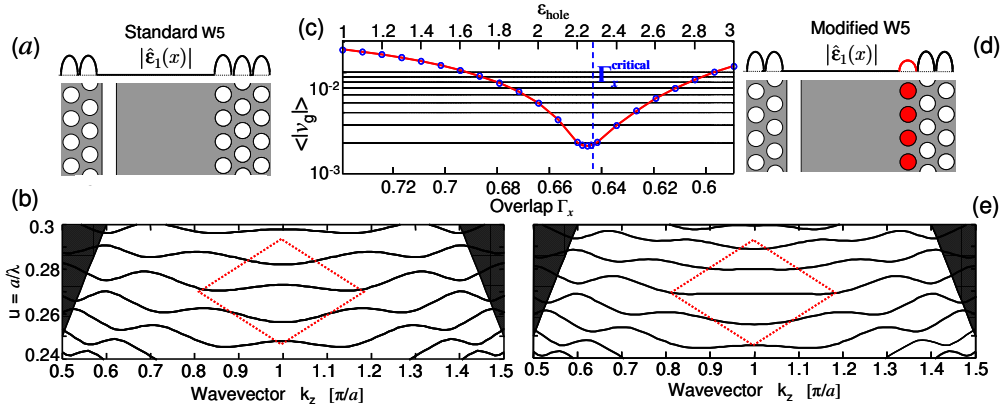


Fig. 7. (a). Standard W5 ST-PhC waveguide and (b) its band diagram and light cone (dark solid regions). (c) Evolution of the average group velocity with the change in hole's dielectric constant, again labeled also by the overlap integral. The group velocity dips close to the expected critical value ≈0.647. (d) W5 ST-PhC waveguide with modified hole dielectric and (e) Flattened band diagram at ε_{hole}=2.25. The flatbands are highlighted in the red lozenge.

3.2 Hole position

Shifting the rows of waveguide boundary holes towards the cladding also leads to the critical regime. Figures 8(a)-8(b) shows a standard W2 ST-PhC waveguide and its dispersion diagram. Lower number of guided modes, and hence anticrossings, in such narrow waveguides lead to intrinsically low band curvatures. Our usual gauge $\langle|\overline{v}_g|\rangle$ becomes in this narrow limit the average velocity of the sole central band enclosed in the red lozenge. As the first row of holes is shifted by an amount $s\times b$, where $b = a\sqrt{3}/2$ is the separation between two adjacent hole rows, the boundary contribution of $\hat{\varepsilon}_1(x)$ is pushed into the cladding, as shown schematically in Fig. 8(d). The overlap Γ_x decreases with the shift, from right to left, as does the average normalized group velocity $\langle|\overline{v}_g|\rangle$. Near the critical overlap

#110813 - $15.00 USD Received 30 Apr 2009; revised 22 May 2009; accepted 23 May 2009; published 4 Aug 2009
(C) 2009 OSA

$\Gamma_x^{\text{critical}}$=1.26, $\langle|\overline{v}_g|\rangle$ drops to around 2.5 times its unperturbed value. The slight deviation between the $\langle|\overline{v}_g|\rangle$ minima and $\Gamma_x^{\text{critical}}$ can be ascribed to the inherent shortcomings of approximate perturbation calculations in high index contrast structures. The wavevector span of flatband can be extended by further modifying the second row of holes, hence the second lobe in the profile of $\hat{\varepsilon}_1(x)$, as demonstrated recently in [11].

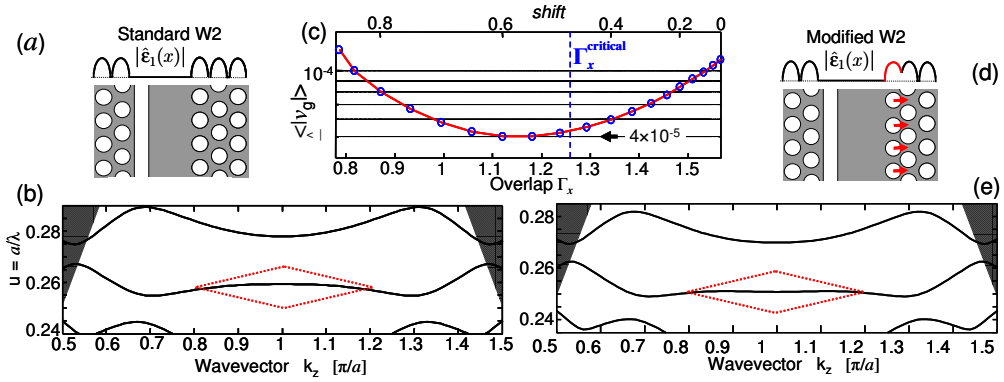


Fig. 8. (a). Standard W2 ST-PhC waveguide and (b) its band diagram with light cone (dark solid regions). (c) Evolution of the average group velocity with the shift in first row of holes labeled by parameter *s* ("shift", see text). The group velocity dips near the critical overlap value. (d) W2 ST-PhC waveguide with modified hole position (e) Flattened band diagram at *s*=0.6. The flatbands are highlighted in the red lozenge.

3.4 Other methods

Several other sophisticated PhC waveguide structures [17, 30-33] have recently been proposed for the slow light engineering. However, here we comment on a few fundamental design aspects in a PhC waveguide and on how they relate to the critical coupling. For instance, changing the width of waveguide [8] has been shown to work for narrow PhC waveguides where the only anticrossing in the PBG, the one near the dielectric band edge, determines the band shape. Due to the influence of the band edge proximity on the coupling strength of this special anticrossing and the fact that the FSR of the single PBG guided mode is elusive, it is delicate to directly test this approach for the critical coupling criteria. Moreover, in broader PhC waveguides, since the mode density in the PBG increases with the width, a similar approach would probably not apply, due to the interaction with other guided modes.

In [14, 15], PhC waveguide cladding symmetry is the design parameter. This method exploits the inversion of mode coupling parity [23] to produce flat dispersion bands. The relative phase of first Fourier contributions $\hat{\varepsilon}_1(x)$ between the two sides of the waveguide is modified. This changes the distribution of coupling strengths among the guided modes, which is no more uniform: two distinct coupling strengths appear having the dependency $(1 \pm \exp[i\Delta\varphi])$ where the phase $\Delta\varphi$ is dictated by the relative shift between cladding positions. One can infer that every other mode has a chance to become flat, so that our approach would have to be generalized to bring more insight. Because it is used by the cited works only in very narrow waveguide (up to W2), there is no chance to witness the systematic aspects of this situation, unlike the bulk of this study on broader waveguides with symmetric $\hat{\varepsilon}_1(x)$.

4. Conclusions

We have described a simple recipe for designing flatbands in a PhC waveguide. The approach is intuitive and based on optimizing the coupling strength of the guided modes to achieve the

#110813 - $15.00 USD Received 30 Apr 2009; revised 22 May 2009; accepted 23 May 2009; published 4 Aug 2009
(C) 2009 OSA

critical coupling regime – the configuration whereby the coupling strength is equivalent to the frequency spacing of the locally equidistant modes. Through CMT and PWE calculations, we demonstrated that a PhC waveguide achieves flatbands around the BZ-edge when its coupling strength reaches its critical value. A prerequisite to our approach is the validity, hitherto unnoticed, of a coupled-mode description of the rich PhC waveguide bandstructure in the entire PBG, carrying features such as the "minigap-stripes" described in [25]. We first determined the default coupling strength of a canonical PhC waveguide that we found to be overcoupled, i.e. the interaction strength of modes is above their critical value. We explicitly assessed this point based on exact simulations. To lower the coupling strength to its critical value, we then optimized the first Fourier harmonic profile $\hat{\varepsilon}_1(x)$ of the periodic waveguide boundary. It was shown that for any optogeometric tuning of the waveguide boundary holes, the slow-down regime was always achieved at the critical coupling. In practice, we made use of a normalized overlap integral Γ_x of non perturbed modes with $\hat{\varepsilon}_1(x)$ of the modified PhC, whose structural parameters were tuned to reach the critical value $\Gamma_x^{\text{critical}}$. The associated collective flatbands were quantified using the average group velocity $\langle|\overline{v}_g|\rangle$: more than one order of magnitude slow down was commonly achieved on average over the substantial zone-edge targeted area of the dispersion diagram. The typical optimization tolerance window has a relative width of a few percent around the exact minimum at $\Gamma_x^{\text{critical}}$. Beyond this point, the bands revert to their original dispersive state. We finally emphasize that our approach gives almost direct rules for the dielectric constant map, similar to the formerly proposed treatment of PhC cavity design [34]. Such approaches drastically reduce the parameter space complexity and the associated lengthy trial-and-error search routines. Lastly, the flatband recipe developed in this work is not just restricted to periodic optical waveguides. It could naturally be extended to analogous electronic structures such as corrugated graphene nanoribbons [35] .

APPENDIX A

A corrugated photonic wire is a perturbed waveguide system wherein the guided modes are in a coupled state with reference to a smooth, non corrugated wire. Away from the critical coupling point, the modes could in general be either *undercoupled,* i.e. $\kappa < \kappa_c$, or *overcoupled*, i.e. $\kappa > \kappa_c$. To achieve flat bands in the former case, the coupling strength has to be increased while it has to be decreased in the later case. In a canonical PhC waveguide defined by omitting one or several rows of holes in a lattice of *identical round-shaped* holes, the dispersion bands are commonly not flat and thus fall in one of the two regimes. To determine which one, we track the evolution of the photonic band structure as a function of the waveguide perturbation. Starting from an almost unperturbed case, a DT-PhC waveguide, a periodic perturbation is gradually introduced until we obtain the standard PhC waveguide, i.e. an ST-PhC waveguide. The reason behind perturbing only one boundary of the DT-PhC waveguide is to easily keep track of the bands and better analyze their formation (see Fig. 5). The band diagram of the W9 equivalent DT-PhC waveguide, calculated by PWE method, is shown is in Fig. 9(b). The dispersion bands are plotted in the first and second BZ to reveal the entire coupling region around the first BZ edge. Moreover for clarity, we only highlight the bands (red) in a fixed interval around the first BZ edge. Since in his case the boundary corrugation is absent, $\kappa \cong 0$ and the dispersion bands can be seen to cross each other, similar to the case of Fig. 3(a).

#110813 - $15.00 USD Received 30 Apr 2009; revised 22 May 2009; accepted 23 May 2009; published 4 Aug 2009
(C) 2009 OSA

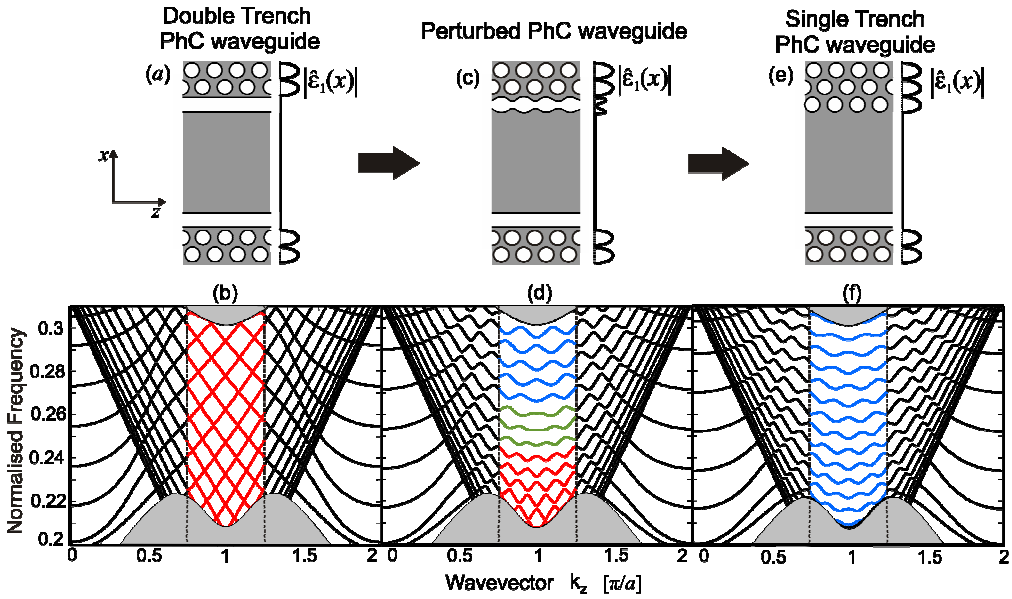


Fig. 9. Evolution of band structure of a PhC waveguide with increasing boundary perturbation; (a,c,e) Sketch of waveguides and dielectric first Fourier harmonic profile, (b,d,f) band structures highlighting the mode coupling region around the BZ edge.

As a periodic sinusoidal perturbation is introduced in one of the boundaries, see Fig. 9(c), curly bands start forming at higher frequencies and gradually progress down to lower frequencies as the perturbation amplitude increases. Figure 9(d) shows the dispersion diagram of this intermediate stage where three distinct families of bands are observed. The red bands at lower frequencies see only a slight perturbation of the boundary and the anticrossings are only beginning to form. At the higher frequency end (blue bands), modes have a greater overlap with the perturbed boundary and hence a higher coupling strength. These two coupling regimes are divided by a third family of modes (highlighted in green) where the band flattening is obvious. We argue that these bands are at the critical coupling point and separate the k-space into overcoupled blue bands with $\kappa > \kappa_c$ and undercoupled red bands with $\kappa < \kappa_c$. Also, the number of band oscillations above the critical region is one less than that below it, as pointed out in Fig. 2. When the boundary perturbation takes the form of round holes, (see Fig. 9(e)), which can be made morphologically continuous, modal coupling increases to a point where only the blue bands exist and the situation of zone edge modes in such a standard PhC waveguide is said to be overcoupled.

#110813 - $15.00 USD Received 30 Apr 2009; revised 22 May 2009; accepted 23 May 2009; published 4 Aug 2009
(C) 2009 OSA